Journal of Alloys and Compounds 690 (2017) 568–574

Contents lists available at ScienceDirect

Journal of Alloys and Compounds

journal homepage: http://www.elsevier.com/locate/jalcom

Elastic, dielectric and electromechanical properties of $(Bi_{0.5}Na_{0.5})TiO_3$-$BaTiO_3$ piezoceramics at the morphotropic phase boundary region

Rodrigo Machado [a, b], Valdeci B. dos Santos [a, c], Diego A. Ochoa [a], Elena Cerdeiras [d], Lourdes Mestres [d], José E. García [a, *]

[a] Departament de Física, Universitat Politècnica de Catalunya - BarcelonaTech, 08034, Barcelona, Spain
[b] Instituto de Física Rosario, Universidad Nacional de Rosario, 2000, Rosario, Argentina
[c] Coordenação de Engenharia de Materiais, Universidade Federal do Piauí, 64049-550, Teresina, Brazil
[d] Departament de Química Inorgànica i Orgànica, Secció de Química Inorgànica, Universitat de Barcelona, 08028, Barcelona, Spain

ARTICLE INFO

Article history:
Received 5 May 2016
Received in revised form
27 July 2016
Accepted 14 August 2016
Available online 16 August 2016

Keywords:
Ceramics
Ferroelectrics
Dielectric response
Piezoelectricity

ABSTRACT

A systematic study of the functional properties of the $(1-x)(Bi_{0.5}Na_{0.5})TiO_3$–$xBaTiO_3$ (BNT-xBT) piezoceramic system for $0.05 \leq x \leq 0.07$ is performed. The samples are obtained through the conventional solid-state route. The expected microstructure for these compounds, with no significant dependence on the composition, is verified by field-emission scanning electron microscopy. The morphotropic phase boundary (MPB) is detected for $x = 0.06$–0.07 by means of the Rietveld analysis of X-ray diffraction data. The dielectric spectra show a frequency-independent, completely diffuse phase transition with a composition-dependent diffusivity coefficient. The depolarization temperature is effectively evaluated from pyroelectric measurements, the value being strongly dependent on the composition. A significant contribution of the extrinsic effect to elastic, dielectric and electromechanical properties is revealed for MPB BNT-xBT. The Bi^{3+} substitution by Ba^{2+} leads to the formation of A-site vacancies, which give rise to the enhancement of domain wall motion, as occurs in other perovskite-type piezoelectrics. Good functional properties are achieved for $x = 0.07$ ($d_{33} = 180$ pC/N), which are similar or even better than those obtained by complex synthesis routes. This system exhibits a remarkable stability in the permittivity that has hitherto not been reported. This fact may open the way for BNT-BT compositions to be used in specific applications in which lead-free piezoceramics have previously been employed with little success, e.g. in high power devices.

1. Introduction

Piezoelectric materials play a key role in electronics, where they are widely used as active element for sensors, actuators, transducers, generators and motors. The most frequently used are the $PbTiO_3$–$PbZrO_3$ (PZT) based materials because they present exceptional piezoresponse [1]. Nonetheless, the problem with these materials is lead toxicity. The new regulations that tend toward removal of lead in the industry make the research for new lead-free piezoceramics a worldwide topic [2].

PZT solid solutions are believed to exhibit great piezoelectric properties for three reasons: (i) the presence of Pb^{2+} with their lone electron pair, which favor hybridization, (ii) the presence of a morphotropic phase boundary (MPB), and (iii) the high contribution of the motion of the ferroelastic domain walls [3]. The search for lead-free compositions with potential high piezoelectric properties has therefore been focused on solid solutions presenting MPB. The $(1-x)(Bi_{0.5}Na_{0.5})TiO_3$–$xBaTiO_3$ system has attracted a great deal of interest because it presents a MPB between the rhombohedral and tetragonal phases (as in the case of PZT) for $x = 0.05$–0.08, where there is a significant enhancement of their dielectric and piezoelectric properties [4–6]. Furthermore, the scientific interest on this system is retained since BNT-based materials seem to be potential candidates for specific applications [2,7,8].

The longitudinal piezoelectric coefficient d_{33} has been reported for undoped BNT-BT system, ranging from 125 pC/N by Takenaka

* Corresponding author.
E-mail address: jose.eduardo.garcia@upc.edu (J.E. García).

http://dx.doi.org/10.1016/j.jallcom.2016.08.116
0925-8388/

et al. [4] up to 200 pC/N by Yilmaz et al. [9]. Improvement of electromechanical properties has been mainly achieved by exploring different sintering methods. Thus, Zhou el al [10]. reported a d_{33} value of 132 pC/N for a sample formed by aqueous gelcasting, whereas Chen et al. [5] obtained a d_{33} value of 176 pC/N for a sample synthesized by the citrate method. The d_{33} value of 200 pC/N was reported in textured ceramics prepared by template grain growth [9]. The enhancement of BNT-BT electromechanical properties has also been extensively explored by doping [11–15], reaching d_{33} values up to 205 pC/N [11]. A careful revision of results of the publications on compositions based on BNT-BT system can be found in a recent review article [16].

Although the biggest contributions to the dielectric and piezoelectric properties of PZT-based materials is the motion of the domain walls [3,17], this subject has not been studied in depth in candidates to replace it [3]. The relevance of the contribution of the domain wall movement evidences the need to study the extrinsic contributions in order to understand how to improve the dielectric and piezoelectric properties in the new lead-free compounds. For this purpose, in this work a systematic study of the functional properties of the BNT-BT system around their MPB is carried out, focusing on the contribution of the extrinsic response to material properties.

2. Experimental procedure

$(1\text{-}x)Bi_{0.5}Na_{0.5}TiO_3$–$xBaTiO_3$ (BNT-xBT) ceramics with $x = 0.05$, 0.06 and 0.07 are prepared by a solid-state reaction route. Bi_2O_3 (99.9%), Na_2CO_3 (99.5%), $BaCO_3$ (99%), and TiO_2 (99.9%) are used as starting raw materials. The raw reagents are weighed according to the desired composition, and then ball-milled with yttria-stabilized zirconia balls in absolute ethanol medium at 300 rpm for 8 h. The solution is first dispersed and then dried. The powders thus obtained are calcined at 700 °C for 2 h and then milled again for 8 h. The final powders are mixed with a binder solution, dried and then pressed at 550 MPa to produce disc-shape (13 mm diameter and 0.5 mm thick) and bar-shape (16 mm long, 4 mm wide and 0.8 mm thick) samples. The pellets are sintered in air at 1200 °C for 2 h in covered platinum crucibles. All as-sintered samples show relative densities over 95% measured by Archimedes' method. Room temperature X-ray diffraction (XRD) patterns of not annealed powder from sintered samples are collected in Bragg-Brentano geometry using a PANalytical X'Pert PRO MPD system with Cu Kα radiation ($\lambda = 1.5406$ Å) and an X'Celerator detector equipped with a focusing primary Ge (111) monochromator. Five repeated scans with a step size of 0.017° and a measuring time of 50 s are acquired for Rietveld analysis. Lattice parameters are refined by global simulation of the full XRD patterns using *Fullprof* program. The samples are polished and a thermal etch for 30 min at 1100 °C is performed in order to evaluate the microstructure that is carried out using a field emission scanning electron microscope, FE-SEM (JEOL JSM-7001F).

Gold electrodes are sputtered on parallel polished faces of the samples for electrical measurements. A precision LCR meter (Agilent E4980A) is used to obtain the real and imaginary parts of the permittivity of unpoled samples at selected frequencies from 100 Hz to 1 MHz. The samples are placed in a closed-loop, cold-finger cryogenic system and in a programmable tubular oven for measurement in a temperature range from −250 °C to 130 °C and from room temperature (RT) to 500 °C, respectively. The ferroelectric hysteresis loops are recorded using a modified Sawyer-Tower circuit at 1 Hz and at RT.

Disc- and bar-shape samples are poled in a silicone bath at 25 °C under a dc electric field of 4 kV/mm for 30 min, and subsequently aged for a week before measurements are taken in order to prevent the influence of aging processes. The static longitudinal piezoelectric coefficient is measured with a d_{33} meter (KCF Technologies PM3500). A precision impedance analyzer (Agilent 4294A) is employed to measure resonance and anti-resonance frequencies of the main vibration extensional mode of bar-shape samples as well as their capacitance value at the frequency where the motional admittance is null, for several selected temperatures in the −250 °C to 130 °C range. The elastic compliance s^E_{11}, the piezoelectric coefficient d_{31}, the stress constant permittivity ε^T_{33} and the electromechanical coupling factor k_{31} are determined on the basis of IEEE standards [18].

Nonlinear dielectric response measurements are carried out in a plane capacitor configuration by using a capacitance comparator bridge specially designed for this type of measurement, as described in detail elsewhere [19]. Permittivity is measured in disc-shape samples by applying a 1 kHz driving ac electric field from 0.06 to 0.6 kV/mm, thereby ensuring a sub-switching range. The pyroelectric response is obtained from the thermally stimulated depolarization current measured by a sub-femtoamperimeter (Keithley 6430) at a heating rate of 5 °C/min from room temperature to above the depolarization temperature.

3. Results and discussion

Fig. 1a shows the XRD patterns for the studied BNT-xBT compositions. Results show pure perovskite structure for all cases and

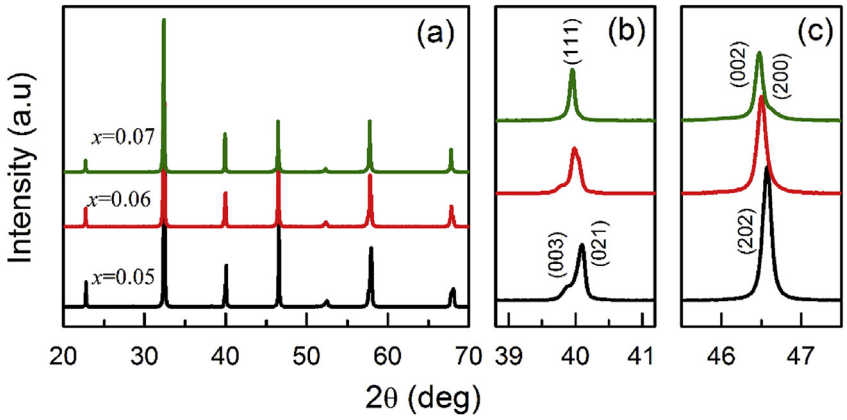

Fig. 1. (a) Normalized X-ray diffraction (XRD) patterns of BNT-xBT ceramics for $x = 0.05$, 0.06 and 0.07. XRD patterns displaying the (b) 39° to 41° and (c) 46° to 47° 2θ regions are also shown. The peak evolution shows the growth of the tetragonal phase at the expense of the rhombohedral one.

Table 1
Phase fraction and lattice parameters obtained from Rietveld refinement of the X-ray diffraction data for single tetragonal and hexagonal lattice formats.

x	Crystal system	Phase fraction (%)	Lattice parameters		Quality of fit	
			a[Å]	c[Å]	Rp (%)	χ^2
0.05	Rhombohedral	94.9	5.50281	13.54524	17.11	6.92
	Tetragonal	5.1	3.89665	3.88273		
0.06	Rhombohedral	58.9	5.50423	13.57572	7.68	3.54
	Tetragonal	41.1	3.90077	3.90188		
0.07	Rhombohedral	48.4	5.52197	13.52650	8.70	4.01
	Tetragonal	51.6	3.90312	3.90556		

no secondary phases are detected. BNT is rhombohedral at room temperature with R3c space group [20]. This symmetry is characterized by a 003/021 peak splitting around $2\theta = 40°$ and a single 202 reflection in the $46° < 2\theta < 47°$ range [5,21]. Fig. 1b and c shows in detail the regions $39° < 2\theta < 41°$ and $45.5° < 2\theta < 47.5°$, respectively. XRD pattern for $x = 0.05$ displays the peaks that characterize the rhombohedral BNT phase. However, when x rises the 003/021 peak splitting, corresponding to a rhombohedral symmetry, evolves to a single 111 reflection, corresponding to a tetragonal symmetry. Furthermore, when x rises the 002/200 tetragonal reflection begins to emerge instead of the 202 rhombohedral reflection. The Rietveld refinement yields a coexistence of rhombohedral and tetragonal phases with 94.9%, 58.9% and 48.4% of rhombohedral phase for $x = 0.05$, 0.06 and 0.07, respectively. These results imply that the MPB region is located for $x = 0.06$ and 0.07, which is in agreement with Refs. [4,22].

Table 1 summarizes the results obtained from the Rietveld refinement. A poor quality of fit is obtained for $x = 0.05$, because the quantity of tetragonal phase required to resolve from conventional XRD data is scarce. Similar fit parameters are obtained when only the rhombohedral phase is considered. Thus, the reported value of the relative percent of the tetragonal phase for this composition is factually inaccurate. Anyway, results from the refinement show clearly that this is not a MPB composition. Fig. 2 shows FE-SEM micrographs of the studied compositions. The images clearly show the polycrystalline structure of the samples with a compact microstructure. The grains are rounded and irregular in shape and inhomogeneous in size, as previously reported for similar compositions [23,24].

The temperature dependent dielectric permittivity for the unpoled BNT-xBT samples are shown in Fig. 3a. Two anomalies, labeled as T_m and T_h, can be identified in the dielectric spectra. The first corresponds to the temperature of the maximum of the dielectric constant and is related to the phase transition between a high symmetry cubic phase and a lower symmetry tetragonal phase [4]. As may be observed, the transition at T_m region is diffuse. The diffusivity degree of the phase transition can be characterized by means of a modified Curie-Weiss equation as follow [25]:

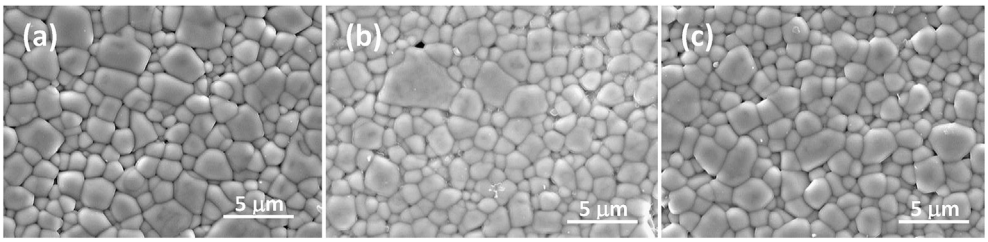

Fig. 2. Field emission scanning electron microscope (FE-SEM) micrographs of BNT-xBT ceramics for (a) $x = 0.05$, (b) $x = 0.06$ and (c) $x = 0.07$. The samples show dense microstructure with irregular shaped grains.

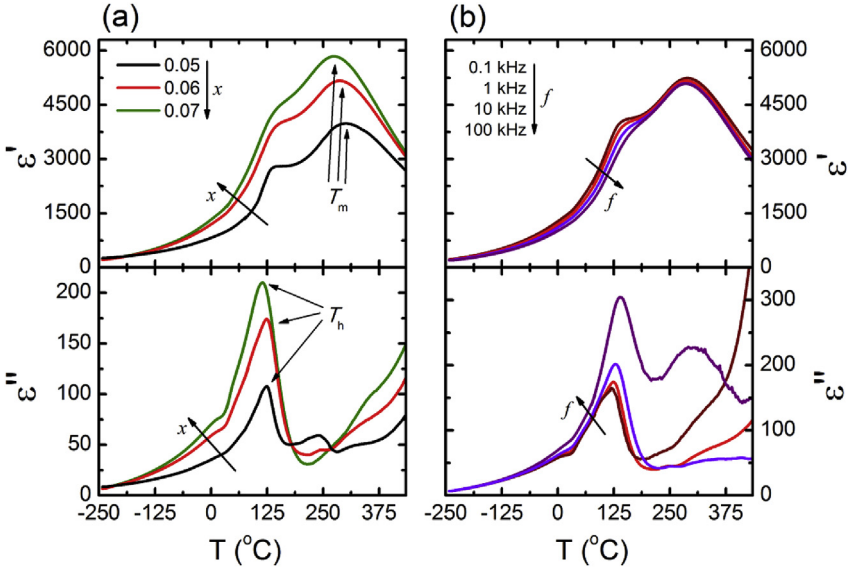

Fig. 3. (a) Temperature dependence of the real and imaginary dielectric permittivity of the unpoled BNT-xBT, for $x = 0.05$, 0.06 and 0.07, at 1 kHz. Two characteristic temperatures, related to the maximum of real (T_m) and imaginary (T_h) permittivity, are identified. (b) Temperature dependence of the real and imaginary dielectric permittivity of BNT-0.06BT at different frequencies. A similar frequency dependence (not shown here) of the dielectric spectra is verified for BNT-0.05BT and BNT-0.07BT.

Table 2
The values of the dielectric constant, ε', and dielectric losses, $tan\delta$, at room temperature as well as the maximum of real permittivity, ε_m, and the temperature, T_m, at which this maximum occurs are extracted from Fig. 3(a). The values of γ and Δ are the fitting parameters obtained from Eq. (1). T_h is extracted from Fig. 3(a) and is the temperature at which the maximum of ε'' occurs, whereas T_d is extracted from Fig. 4 and is the value of the temperature at which the macroscopic polarization is 10% of their initial value.

x	ε'	$tan\delta$ (%)	ε_m	T_m (°C)	γ	Δ (°C)	T_h (°C)	T_d (°C)
0.05	940	4.2	3982	300	2.00	177	123	115
0.06	1397	4.6	5182	289	1.92	180	124	95
0.07	1557	5.0	5830	273	1.92	195	114	66

$$\varepsilon' = \frac{\varepsilon_m}{1 + \left(\frac{T - T_m}{\Delta}\right)^{\gamma}} \quad (1)$$

where ε_m is the maximum of the dielectric permittivity, γ indicates the character of the phase transition (being $1 \leq \gamma \leq 2$ such that $\gamma = 1$ indicates a normal phase transition; $\gamma = 2$ denotes a 'complete' diffuse phase transition), and Δ is a measure of the peak broadening and is regarded as the diffusivity coefficient. The computed values of γ and Δ are given in Table 2. Results reveal that this phase transition is completely diffuse for all compositions. A diffuse phase transition in ferroelectrics occurs as a consequence of a structural disorder that breaks the translational invariance of the lattice [26]. Here, the origin of the diffusive character of the phase transition may derive from the fact that different cations, Na^{+}, Ba^{2+} and Bi^{3+}, occupy the A-site at the perovskite, leading to local compositional fluctuations [24,27]. Thus, a Curie point distribution is generated [28]. This may also explain the increase in Δ with the Ba content, since Δ is directly related to the disorder of the perovskite structure [25,26].

The increase in the Ba content lowers the T_m and enhances the ε_m, as can be seen in Fig. 3a and reported in Table 2. The increase in ε_m is a feature that is in agreement with a large number of other works [21,24,29–32]. However, the behavior of T_m seems to be preparation-related, because the opposite trend [32] and even an almost invariant T_m [24] have been also reported. Fig. 3b shows that the value of T_m is frequency independent, indicating a non-relaxor phase transition. This fact is a common feature for all the compositions under study.

The second anomaly of the dielectric spectra of BNT-xBT manifests as a hump in the real permittivity at T_h that corresponds with a peak in the imaginary permittivity. This anomaly is commonly associated to a ferroelectric-antiferroelectric phase transition. The BNT-BT system evolves around T_h towards a phase that has been reported as antiferroelectric tetragonal [24,30,32]. The hump of ε' and the peak of ε'' are both frequency dependent, as can be seen in Fig. 3b. This feature, together with transmition electron microscopy (TEM) studies, lead some researchers to use the term "antiferroelectric relaxor" to refer to the phase for $T > T_h$ [30,33]. However, the antiferroelectric phase is not unanimously accepted [22,34]. The temperature T_h is taken frequently as the depolarization temperature [32,35], although its value cannot be effectively established from the permittivity versus temperature curve. Here, the pyroelectric response is measured in order to estimate the depolarization temperature T_d for each composition. Fig. 4 shows the temperature dependence of the macroscopic polarization for the studied samples. As can be observed, the polarization drops abruptly at a given temperature depending on composition. The values of T_h and T_d are shown in Table 2. It is important to point out that: (i) T_d is significantly lower than T_h, and (ii) T_d is strongly dependent on the BT content. Consequently, an accurate estimation of the depolarization temperature should not be carried out by means of the dielectric response.

Recalling Fig. 3a, one is able to see that both the real and imaginary permittivity are very similar at low temperatures for all compositions. At low temperatures, the domain walls freeze and only the intrinsic (lattice) response contributes to permittivity [17]. The intrinsic permittivity appears not to depend significantly on the BT content in the BNT-xBT system around MPB, although it is well known that lattice response depends on the crystallographic structure [36]. At higher temperatures, the observed differences in the permittivity are a manifestation of the domain wall contribution. Comparison of the values of real permittivity at room temperature with those of very low temperature (30 K) at 1 kHz lead to the conclusion that the extrinsic contribution enhances real permittivity from ~260% for $x = 0.05$–~600% for $x = 0.07$. The Ba^{2+} is a more likely substitute for Bi^{3+} because its radii are closer and because of energy considerations [21]. This substitution generates A-site vacancies, thereby increasing the domain wall mobility, and as a result the dielectric permittivity rises and the coercive field is lowered, as is reported for the PZT system when it is doped with donor (softener) cations [37,38].

Fig. 5 shows the room temperature P-E hysteresis loops at 1 Hz. As may be observed, the addition of BT lowers the coercive field as expected, while the remanent polarization remains unchanged.

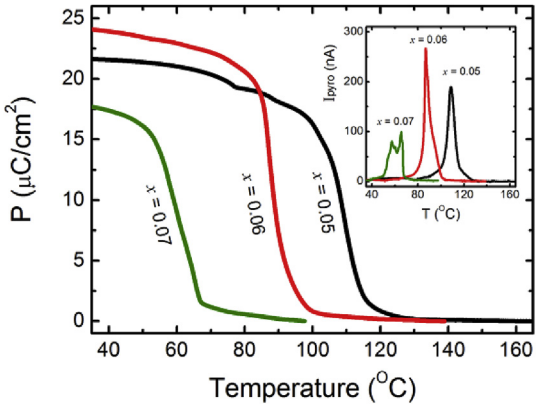

Fig. 4. Temperature dependence of the macroscopic polarization of the BNT-xBT, for $x = 0.05$, 0.06 and 0.07, computed from the integral of the pyroelectric current. The polarization fall corresponds with a sharp peak in the pyroelectric current, which are shown in the inset.

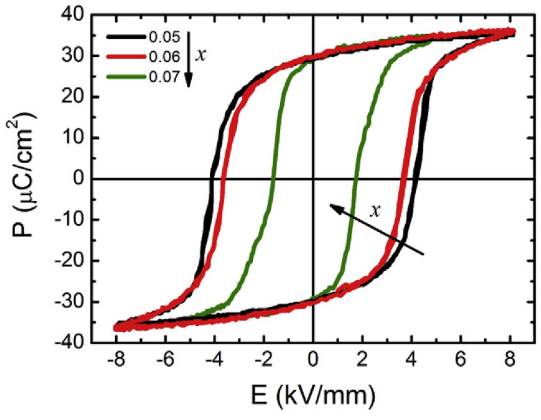

Fig. 5. Electric field-induced polarization hysteresis loops of BNT-xBT ceramics for (a) $x = 0.05$, (b) $x = 0.06$ and (c) $x = 0.07$. Typical ferroelectric hysteresis loops are displayed for all compositions. A significant drop in the coercive field is observed for $x = 0.07$.

Table 3
Room temperature values of the elastic compliance s^E_{11}, the piezoelectric coefficient d_{31}, the electromechanical coupling factor k_{31} and the real permittivity at stress constant ε^T_{33}, extracted from the data in Fig. 6. The remanent polarization P_r and the coercive field E_c are extracted from Fig. 5. The reported longitudinal static piezoelectric coefficient d_{33} is measured by using a d_{33} meter at room temperature.

x	d_{33} (pC/N)	ε^T_{33}	d_{31} (pC/N)	s^E_{11} (10^{-12}/Pa)	k_{31}	P_r (μC/cm^2)	E_c (kV/mm)
0.05	123	499	26	7.2	0.14	30	4.1
0.06	147	525	34	8.5	0.17	30	3.6
0.07	180	698	37	8.0	0.17	30	1.6

Indeed, the coercive field drops notably from 4.1 kV/mm for $x = 0.05$ to 1.6 kV/mm for $x = 0.07$ (Table 3). A downfall of the coercive field could be explained as a result of the phase coexistence in MPB systems where the polarization rotation phenomenon maximizes, thereby facilitating the polarization switching. However, this effect cannot explain by itself the difference in the coercive field value for $x = 0.06$ and 0.07. Thus, the increase in the domain wall mobility, as will be verified from the Rayleigh analysis, seems to be the main effect leading to the lowering of the coercive field for $x = 0.07$. Note that the remanent polarization obtained by pyroelectric measurement (Fig. 4) is lower than the obtained by *P-E* measurement (Fig. 5). This is produced by aging effect; i.e., generally, ferroelectric materials are not capable to retain the total remanent polarization because of the stress release and other microscopic effects. This effect appears to be dependent of BT content for BNT-BT system since different values of the room temperature polarization are exhibited.

In MPB systems, the flattening of the free energy profile favors the polarization rotation mechanism, thus giving rise to the enhancement of the properties at this region [39–41]. It is believed that such kind of phase coexistence permits an almost continuous rotation of the polarization vector under an external electric field, producing an enhancement of the piezoelectric response. In fact, this is the main intrinsic mechanism for the improvement of the electromechanical properties at the MPB [42]. Table 3 shows the enhancement of the piezoelectric properties in MPB BNT-*x*BT. The static longitudinal piezoelectric coefficient d_{33} enhances from 123 pC/N for $x = 0.05$ to 180 pC/N for $x = 0.07$. The combined effect of the domain wall mobility and the polarization rotation may be the reason for this improvement. The d_{33} values are obtained under the poling conditions mentioned above (Experimental section). Nevertheless, the d_{33} of the samples after measurement of their hysteresis loop at 1 Hz turns out to be the same as that obtained under poling conditions; i.e., the electric field produced during the hysteresis loop is sufficient for such a short time. In the BNT-BT system, the flattening of the free energy at the MPB seems to favor the rotation of the polarization in such a manner that it is then not necessary to perform an intensive poling. To our knowledge, the d_{33} obtained for $x = 0.07$ (180 pC/N) is the highest reported value of d_{33} in the undoped BNT-BT system synthesized by a solid-state reaction route.

The temperature dependence of the elastic compliance s^E_{11}, the piezoelectric coefficient d_{31}, the electromechanical coupling factor k_{31} and the dielectric constant ε^T_{33} are shown in Fig. 6 in order to evaluate the BNT-*x*BT performance over a wide temperature range. Properties are measured until depolarization temperature is reached for each composition. As can be observed, the properties increase notably as the temperature rises. For instance, d_{31} increases from low temperature to room temperature by almost 300% in the case of $x = 0.06$ and 0.07, and by 200% for $x = 0.05$ (Fig. 6b). The properties increase may be explained because the domain wall motion is a thermally activated phenomenon. From a broader perspective, the extrinsic contribution (defined as all responses that are different from the intrinsic response) appears to be a major

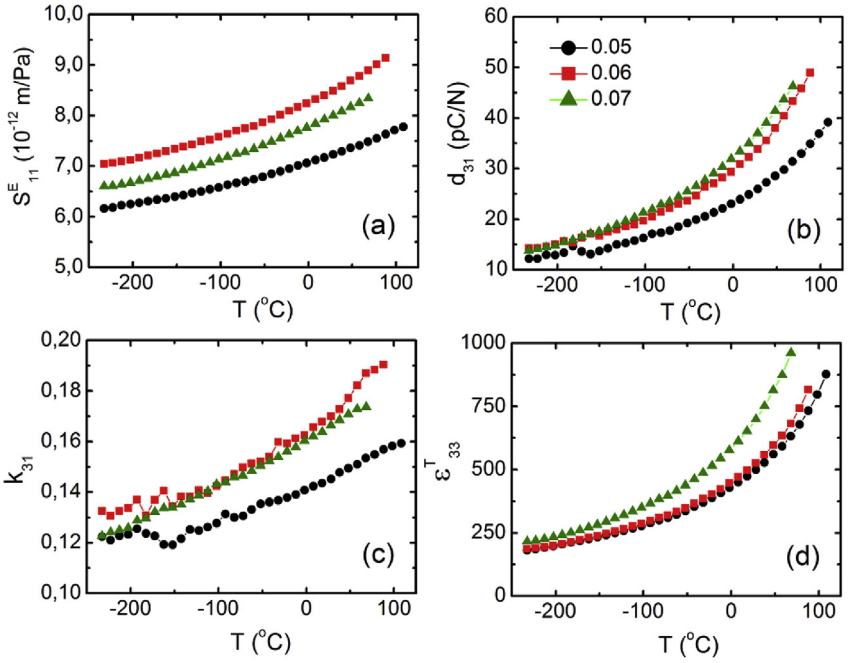

Fig. 6. Temperature dependence of (a) the elastic compliance s^E_{11}, (b) the piezoelectric coefficient d_{31}, (c) the electromechanical coupling factor k_{31} and (d) the real permittivity at stress constant ε^T_{33} of BNT-*x*BT, for $x = 0.05$, 0.06 and 0.07.

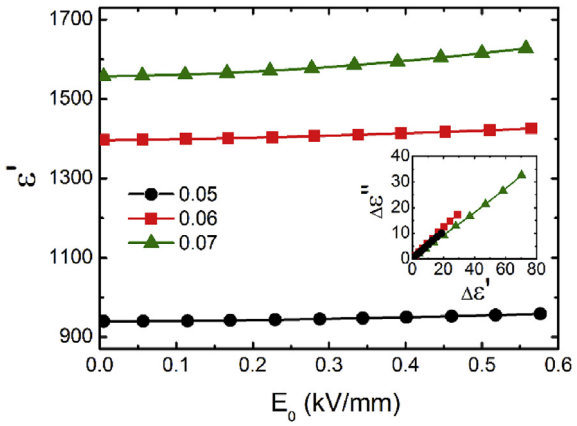

Fig. 7. Real dielectric permittivity as a function of the amplitude of the applied ac electric field of BNT-*x*BT, for $x = 0.05$, 0.06 and 0.07. The inset shows the relation between the increments of the imaginary ($\Delta\varepsilon''$) and real ($\Delta\varepsilon'$) parts of the relative permittivity for all compositions.

contribution to the dielectric, mechanical and electromechanical properties of MPB BNT-*x*BT at room temperature. Table 3 shows the values of the measured properties at room temperature. Good properties for the undoped BNT-BT system are obtained for $x = 0.07$, although it exhibits a low depolarization temperature.

It is widely accepted that in perovskite polycrystals the extrinsic contribution is mainly due to domain wall motion [17]. Here, nonlinear dielectric measurement is performed in order to study the domain wall motion dynamics in term of Rayleigh's law. In this model it is assumed that the increment in the real ε' as well as the imaginary ε'' relative permittivity linearly depends on the amplitude E_0 of the applied ac electric field, as follows [43]:

$$\varepsilon' = \varepsilon_L + \alpha E_0 \tag{2}$$

$$\varepsilon'' = \frac{4}{3\pi}\alpha E_0 \tag{3}$$

where ε_L is the real part of the relative permittivity (i.e. the dielectric constant) at zero-field amplitude, and α is the Rayleigh coefficient that is directly related to the magnitude of the nonlinear response. Fig. 7 shows the dielectric constant as a function of E_0 for all BT concentrations. As can be observed, ε' increases slightly as the amplitude of the electric field increases. Taking as a reference the increase in the dielectric constant at $E_0 = 0.3$ kV/mm, the biggest increase in BNT-*x*BT is 1.4% for $x = 0.07$, while it is 35% and 50% in a well-known KNN composition [44] and a soft commercial PZT (Pz27, from Ferroperm A/S) [19], respectively. In fact, the increment of the dielectric constant in a hard commercial PZT (PZT4, from Morgan Matroc Ltd.) is 6% at $E_0 = 0.3$ kV/mm [19]. It is important to point out that hard PZT materials are the commercial piezoceramics exhibiting the highest properties stability. Hence, the results indicate that the BNT-BT system exhibits a high stability in the dielectric response, which is not a common feature in lead-free piezoelectric compositions.

As a result of Eqs. (2) and (3), the ratio m_ε between the value of the imaginary and real increments of permittivity is a constant that does not depend on the material; i.e. $m_\varepsilon = \Delta\varepsilon''/\Delta\varepsilon' = 4/3\pi$ ($m_\varepsilon \approx 0.42$). The inset in Fig. 7 shows the $\Delta\varepsilon''$ versus $\Delta\varepsilon'$ curves for the three BT concentrations. A linear relation is obtained in all cases, as predicted by the Rayleigh model. The values of m_ε are 0.53, 0.60 and 0.46 for $x = 0.05$, 0.06 and 0.07, respectively. These values are higher than those predicted by the Ryleigh model, which is not a behavior peculiar to the BNT-BT system. Values of m_ε higher than 0.42 are obtained in other perovskite piezoceramics such as PLZT ($m_\varepsilon = 0.51$) [45] and PMN-35PT ($m_\varepsilon = 0.70$) [46]. These results indicate that the increment of the dielectric losses is higher than that expected in the model; i.e., dissipative processes exist that are not taken into account by the model. This could be explained by field-induced phenomena such as conductive processes, which are not related to domain wall motion. In this context, the BT content dependence of m_ε value could be due to that conductive phenomena affect differently each composition; for instance, because of the slight differences in the density.

4. Conclusions

The morphotropic phase boundary of the obtained (1-*x*)($Bi_{0.5}Na_{0.5}$)TiO_3–*x*$BaTiO_3$ (BNT-*x*BT) piezoceramics is detected for $x = 0.06$–0.07 as a mixture of rhombohedral and tetragonal phases, which are quantified by Rietveld analysis. To our knowledge, the obtained piezoelectric coefficient for $x = 0.07$ ($d_{33} = 180$ pC/N) is the highest reported value of d_{33} in the undoped BNT-BT system synthesized by a solid state reaction route. The temperature dependence of the dielectric response shows two anomalies that are a common feature in MPB BNT-*x*BT. One of these anomalies seems to be associated to a transition from a polar to a nonpolar state of the material, which is commonly linked to a ferroelectric-antiferroelectric phase transition. Here, the real depolarization temperatures are evaluated from pyroelectric measurements and show a strong compositional dependence. The observed stability of dielectric properties opens up the possibility of exploring the viability of this system for its use in specific high power applications once the losses are minimized. Furthermore, these materials are capable of acquiring their piezoelectric properties by applying a dc electric field for a short time, which could be technologically important for a possible massive production of BNT-BT-based piezoceramics due to the energy saving involved.

Acknowledgements

This work is supported by the MINECO (Spanish Government) project MAT2013-48009-C4-2-P. Dr. R.Machado and Dr. V.B dos Santos thank CONICET and CNPq, respectively, for their post-doctoral scholarships.

References

[1] S. Priya, S. Nahm (Eds.), Lead-Free Piezoelectrics, Springer, New York, 2012.
[2] J. Rödel, K. Webber, R. Dittmer, W. Jo, M. Kimura, D. Damjanovic, Transferring lead-free piezoelectric ceramics into application, J. Eur. Ceram. Soc. 35 (2015) 1659.
[3] D. Damjanovic, N. Klein, J. Li, V. Porokhonskyy, What can be expected from lead-free piezoelectric materials? Funct. Mater. Lett. 3 (2010) 5.
[4] T. Takenaka, K. Maruyama, K. Sakata, ($Bi_{1/2}Na_{1/2}$)TiO_3-$BaTiO_3$ system for lead-free piezoelectrics ceramics, Jpn. J. Appl. Phys. 30 (1991) 2236.
[5] M. Chen, Q. Xu, B.H. Kim, B.K. Ahn, J.H. Ko, W.J. Kang, O.J. Nam, Structure and electrical properties of ($Na_{0.5}Bi_{0.5}$)$_{1-x}Ba_xTiO_3$ piezoelectric ceramics, J. Eur. Ceram. Soc. 28 (2008) 843.
[6] G. Picht, J. Töpfer, E. Hennig, Structural properties of ($Bi_{0.5}Na_{0.5}$)$_{1-x}Ba_xTiO_3$ lead-free piezoelectric ceramics, J. Eur. Ceram. Soc. 30 (2010) 3445.
[7] W.-S. Kang, J.-H. Koh, (1−x)$Bi_{0.5}Na_{0.5}TiO_3$–x$BaTiO_3$ lead-free piezoelectric ceramics for energy-harvesting applications, J. Eur. Ceram. Soc. 35 (2015) 2057.
[8] J. Zhang, L. Sun, X.-Y. Geng, B.-B. Zhang, G.-L. Yuan, S.-T. Zhang, Temperature dependent structures and properties of $Bi_{0.5}Na_{0.5}TiO_3$-based lead free piezoelectric composite, Dalton Trans. 45 (2016) 10891.
[9] H. Yilmaz, S. Trolier-McKinstry, G. Messing, (Reactive) Templated grain growth of textured sodium bismuth titanate ($Na_{1/2}Bi_{1/2}TiO_3$-$BaTiO_3$) ceramics—II Dielectric and piezoelectric properties, J. Electroceram 11 (2003) 217.
[10] D. Zhou, H. Li, S. Gong, Y. Hu, K. Han, Sodium bismuth titanate-based lead-free piezoceramics prepared by aqueous gelcasting, J. Am. Ceram. Soc. 91 (2008) 2792.
[11] T.-S. Zhou, R.-X. Huang, X.-Z. Shang, F. Peng, J.-Y. Guo, L.-Y. Chai, H.-S. Gu, Lead-free In_2O_3-doped ($Bi_{0.5}Na_{0.5}$)$_{0.93}Ba_{0.07}TiO_3$ ceramics synthesized by

direct reaction sintering, Appl. Phys. Lett. 90 (2007) 182903.
[12] P. Fu, Z. Xu, R. Chu, W. Li, G. Zang, J. Hao, Piezoelectric, ferroelectric and dielectric properties of Nd_2O_3-doped $(Bi_{0.5}Na_{0.5})_{0.94}Ba_{0.06}TiO_3$ lead-free ceramics, Mater. Sci. Eng. B 167 (2010) 161.
[13] P. Fu, Z. Xu, R. Chu, W. Li, G. Zang, J. Hao, Piezoelectric, ferroelectric and dielectric properties of La_2O_3-doped $(Bi_{0.5}Na_{0.5})_{0.94}Ba_{0.06}TiO_3$ lead-free ceramics, Mater. Des. 31 (2010) 796.
[14] P. Fu, Z. Xu, R. Chu, W. Li, G. Zang, J. Hao, Piezoelectric, ferroelectric and dielectric properties of Sm_2O_3-doped $(Bi_{0.5}Na_{0.5})_{0.94}Ba_{0.06}TiO_3$ lead-free ceramics, Mater. Chem. Phys. 124 (2010) 1065.
[15] P. Fu, Z. Xu, R. Chu, W. Li, Q. Xie, Y. Zhang, Q. Chen, Effect of Dy_2O_3 on the structure and electrical properties of $(Bi_{0.5}Na_{0.5})_{0.94}Ba_{0.06}TiO_3$ lead-free piezoelectric ceramics, J. Alloy. Compd. 508 (2010) 546.
[16] M.E. Villafuerte-Castrejón, E. Morán, A. Reyes-Montero, R. Vivar-Ocampo, J.-A. Peña-Jiménez, S.-O. Rea-López, L. Pardo, Towards lead-free piezoceramics: facing a synthesis challenge, Materials 9 (2016) 21.
[17] Q.M. Zhang, H. Wang, N. Kim, L.E. Cross, Direct evaluation of domain-wall and intrinsic contributions to the dielectric and piezoelectric response and their temperature dependence on lead zirconate-titanate ceramics, J. Appl. Phys. 75 (1994) 454.
[18] ANSI/IEEE Std. 176, IEEE Standard on Piezoelectricity, IEEE, 1978.
[19] J.E. García, R. Pérez, A. Albareda, High electric field measurement of dielectric constant and losses of ferroelectric ceramics, J. Phys. D. Appl. Phys. 34 (2001) 3279.
[20] G.O. Jones, P.A. Thomas, Investigation of the structure and phase transitions in the novel A-site substituted distorted perovskite compound $Na_{0.5}Bi_{0.5}TiO_3$, Acta Crystallogr. Sect. B Struct. Sci. 58 (2002) 168.
[21] B. Parija, T. Badapanda, S. Panigrahi, T.P. Sinha, Ferroelectric and piezoelectric properties of $(1-x)(Bi_{0.5}Na_{0.5})TiO_3-xBaTiO_3$ ceramics, J. Mater. Sci. Mater. Electron 24 (2013) 402.
[22] B. Chu, D. Chen, G. Li, Q. Yin, Electrical properties of $Na_{1/2}Bi_{1/2}TiO_3-BaTiO_3$ ceramics, J. Eur. Ceram. Soc. 22 (2002) 2115.
[23] B. Parija, T. Badapanda, P.K. Sahoo, M. Kar, P. Kumar, S. Panigrahi, Structural and electromechanical study of $(Bi_{0.5}Na_{0.5})TiO_3-BaTiO_3$ solid-solutions, Proc. Appl. Ceram. 7 (2013) 73.
[24] C. Xu, D. Lin, K.W. Kwok, Structure, electrical properties and depolarization temperature of $(Bi_{0.5}Na_{0.5})TiO_3$-$BaTiO_3$ lead-free piezoelectric ceramics, Solid State Sci. 10 (2008) 934.
[25] I.A. Santos, J.A. Eiras, Phenomenological description of the diffuse phase transition in ferroelectrics, J. Phys. Condens. Matter 13 (2001) 11733.
[26] D. Viehland, S.J. Jang, L.E. Cross, M. Wuttig, Local polar configurations in lead magnesium niobate relaxors, J. Appl. Phys. 69 (1991) 414.
[27] Q. Xu, Y.-H. Huang, M. Chen, W. Chen, B.-H. Kim, B.-K. Ahn, Effect of bismuth deficiency on structure and electrical properties of $(Na_{0.5}Bi_{0.5})_{0.93}Ba_{0.07}TiO_3$ ceramics, J. Phys. Chem. Solids 69 (2008) 1996.
[28] B.E. Vugmeister, H. Rabitz, Coexistence of the critical slowing down and glassy freezing in relaxor ferroelectrics, Phys. Rev. B 61 (2000) 14448.
[29] Y. Hiruma, H. Nagata, T. Takenaka, Phase transition temperatures and piezoelectric properties of $(Bi_{1/2}Na_{1/2})TiO_3-(Bi_{1/2}K_{1/2})TiO_3-BaTiO_3$ lead-free piezoelectric ceramics, Jpn. J. Appl. Phys. 45 (2006) 7409.
[30] C. Ma, X. Tan, Phase diagram of unpoled lead-free $(Bi_{1/2}Na_{1/2})TiO_3-BaTiO_3$ ceramics, Solid State Commun. 150 (2010) 1497.
[31] F. Cordero, F. Craciun, F. Trequattrini, E. Mercadelli, C. Galassi, Phase transitions and phase diagram of the ferroelectric perovskite $(Na_{0.5}Bi_{0.5})_{1-x}Ba_xTiO_3$ by anelastic and dielectric measurements, Phys. Rev. B 81 (2010) 144124.
[32] T. Oh, M.-H. Kim, Phase relation and dielectric properties in $(Bi_{1/2}Na_{1/2})_{1-x}Ba_xTiO_3$ lead-free ceramics, Mater. Sci. Eng. B 132 (2006) 239.
[33] C. Ma, X. Tan, E. Dul'kin, M. Roth, Domain structure-dielectric property relationship in lead-free (1-x)$(Bi_{1/2}Na_{1/2})TiO_3$-x$BaTiO_3$ ceramics, J. Appl. Phys. 108 (2010) 104105.
[34] T. Takenaka, H. Nagata, Y. Hiruma, Phase transition temperatures and piezoelectric properties of $(Bi_{1/2}Na_{1/2})TiO_3$- and $(Bi_{1/2}K_{1/2})TiO_3$-based bismuth perovskite lead-free ferroelectric ceramics, IEEE Trans. Ultrason. Ferroelectr. Freq. Control 56 (2009) 1595.
[35] K. Pengpat, S. Hanphimol, S. Eitssayeam, U. Intatha, G. Rujijanagul, T. Tunkasiri, Morphotropic phase boundary and electrical properties of lead-free bismuth sodium lanthanum titanate-barium titanate ceramics, J. Electroceram 16 (2006) 301.
[36] X.L. Zhang, Z.X. Chen, L.E. Cross, W.A. Schulze, Dielectric and piezoelectric properties of modified lead zirconate titanate ceramics from 4.2 to 300 K, J. Mater. Sci. 18 (1983) 968.
[37] R. Gerson, Variation in ferroelectric characteristics of lead zirconate titanate ceramics due to minor chemical modifications, J. Appl. Phys. 31 (1960) 188.
[38] A. Pramanick, D. Damjanovic, J.E. Daniels, J.C. Nino, J.L. Jones, Origins of electro-mechanical coupling in polycrystalline ferroelectrics during subcoercive electrical loading, J. Am. Ceram. Soc. 94 (2011) 293.
[39] H. Fu, R.E. Cohen, Polarization rotation mechanism for ultrahigh electromechanical response in single-crystal piezoelectrics, Nature 403 (2000) 281.
[40] D. Damjanovic, Comments on origins of enhanced piezoelectric properties in ferroelectrics, IEEE Trans. Ultrason. Ferroelectr. Freq. Control 56 (2009) 1574.
[41] M. Ogino, Y. Noguchi, Y. Kitanaka, M. Miyayama, C. Moriyoshi, Y. Kuroiwa, Polarization rotation and monoclinic distortion in ferroelectric $(Bi_{0.5}Na_{0.5})TiO_3-BaTiO_3$ single crystals under electric fields, Crystals 4 (2014) 273.
[42] D. Damjanovic, A morphotropic phase boundary system based on polarization rotation and polarization extension, Appl. Phys. Lett. 97 (2010) 062906.
[43] J.E. Garcia, R. Perez, A. Albareda, Contribution of reversible processes to the non-linear dielectric response in hard lead zirconate titanate ceramics, J. Phys. Condens. Matter 17 (2005) 7143.
[44] D.A. Ochoa, J.E. García, R. Perez, V. Gomis, A. Albareda, F. Rubio-Marcos, J.F. Fernandez, Extrinsic contribution and non-linear response in lead-free KNN-modified piezoceramics, J. Phys. D. Appl. Phys. 42 (2009) 025402.
[45] E. Perez-Delfin, J.E. Garcia, D.A. Ochoa, R. Perez, F. Guerrero, J.A. Eiras, Effect of Mn-acceptor dopant on dielectric and piezoelectric responses of lead lanthanum zirconate titanate piezoceramics, J. Appl. Phys. 110 (2011) 034106.
[46] J.E. García, J.D.S. Guerra, E.B. Araújo, R. Pérez, Domain wall contribution to dielectric and piezoelectric responses in $0.65Pb(Mg_{1/3}Nb_{2/3})-0.35PbTiO_3$ ferroelectric ceramics, J. Phys. D. Appl. Phys. 42 (2009) 115421.